TIMED Doppler Interferometer (TIDI)

Timothy L. Killeen, Wilbert R. Skinner,* Roberta M. Johnson, Charles J. Edmonson, Qian Wu, Rick J. Niciejewski, Heinz J. Grassl, David A. Gell, Peter E. Hansen, Jon D. Harvey, and Julie F. Kafkalidis

Space Physics Research Laboratory, Department of Atmospheric, Oceanic, and Space Sciences
The University of Michigan, Ann Arbor, Mi. 48109-2143

ABSTRACT

The TIMED Doppler Interferometer (TIDI) is a Fabry-Perot interferometer designed to measure winds, temperatures, and constituents in the mesosphere and thermosphere (60-300 km) region of the atmosphere as part of the TIMED mission. TIDI is a limb viewer and observes emissions from OI 557.7 nm, OI 630.0 nm, OII 732.0 nm, O_2(0-0), O_2(0-1), Na D, OI 844.6 nm, and OH in the spectral region 550-900 nm. Wind measurement accuracies will approach 3 ms^{-1} in the mesosphere and 15 ms^{-1} in the thermosphere. The TIDI instrument has several novel features that allow high measurement accuracies in a modest-sized instrument. These include: an optical system that simultaneously feeds the views from four scanning telescopes which are pointed at ±45° and ±135° to the spacecraft velocity vector into a high-resolution interferometer, the first spaceflight application of the circle-to-line imaging optic (CLIO), and a high quantum efficiency, low noise CCD.

Keywords: Fabry-Perot interferometers, remote sensing, wind measurements

1. INTRODUCTION

The TIMED Doppler Interferometer (TIDI) will investigate the dynamics and energetics of the Earth's mesosphere and lower thermosphere-ionosphere (MLTI) from an altitude of 60 to 300 km as part of the TIMED mission.[1] TIDI measurements will obtain a global description of the vector wind and temperature fields, as well as important information on gravity waves, species densities, airglow and auroral emission rates, noctilucent clouds, and ion drifts. TIDI will provide basic information about global winds and temperatures. TIDI will also contribute to the study of MLTI energetics. Some of the key TIDI parameters are shown in Table 1.

Table 1. TIDI parameters

Spacecraft altitude	625 km
Orbital inclination	74.1º
Time to precess through 24 hours of local time	120 days
Instrument mass	41.8 kg
Electrical Power	19.32 watts (orbit ave.)
Heater Power	11.0 watts
Data Rate	2494 bits/s
Altitude Resolution	2 km
Spectral Range	550 - 900 nm
Lifetime	>2 years
Operational temperature	20±5°C for profiler
	-80°C for detector
	-20°C to 40°C for telescopes
Retrieved quantities	vector wind field, temperature, and some constituent densities from 60 to 120 km

The TIDI interferometer (or Profiler) primarily measures horizontal vector winds and neutral temperatures from 60 to 300 km, with a vertical resolution of ~2 km at the lower altitudes and with accuracies that approach ~3 m/s and ~2 K, respectively, under optimum viewing conditions. The TIDI design allows for 100% duty cycle instrument operation during daytime, nighttime, and in auroral conditions. TIDI is a limb viewer and observes emissions from OI at 557.7 nm, OI at 630.0 nm, OII at 732.0 nm, O_2(0-0) at 762 nm, O_2(0-1) at 861 nm, Na D at 589 nm, OI at 844.6 nm, and OH to determine Doppler wind and temperature throughout the TIMED altitude range. TIDI also makes spectral ratio observations to determine O_2 densities and rotational temperatures.

*Correspondence: Email: wskinner@umich.edu; Telephone: 734 647 3960; Fax: 734 763 7130

TIDI is a direct descendent of other spaceflight Fabry-Perot interferometers built at the Space Physics Research Laboratory of the University of Michigan. The first instrument was the Dynamics Explorer Fabry-Perot Interferometer (DE-FPI) which was a single-etalon instrument designed for observations of emissions from the thermosphere.[2] It was launched in 1981 and operated for 18 months until the satellite re-entered the Earth's atmosphere. The High Resolution Doppler Imager flying on the Upper Atmosphere Research Satellite (HRDI/UARS) is a triple-etalon Fabry-Perot system designed for observations of the stratosphere, mesosphere, and lower thermosphere (10-120 km).[3,4] It was launched in 1991 and is still operating at the time of this writing. The TIDI instrument uses designs and concepts developed in these programs while incorporating new ideas and technologies. This paper will discuss the optical design of the TIDI instrument and summarize the performance of many of the optical components. Other important aspects of the instrument such as the mechanical and thermal design, and instrument operations are beyond the scope of this paper. At this writing, the complete TIDI calibration is not complete, so it is not possible to provide a complete description of the end-to-end performance. However, some metrics will be provided to indicate the type of performance expected from this instrument.

2. INSTRUMENT OVERVIEW

TIDI comprises three major subsystems: four identical telescopes, a Fabry-Perot interferometer with a CCD detector, and an electronics box (Figure 1). Light from the selected regions of the atmosphere is collected by the telescopes which are fiber-optically coupled to the detection optics. The four fields of view are spatially scrambled by the random distribution of the fibers in the bundle. A fifth field from a calibration deck is combined with the others so the input to the profiler consists of an array of five concentric circular 90 degree wedges. This input is collimated for transmission through a selected filter, followed by a Fabry-Perot etalon, and is finally imaged onto a CCD via a Cassegrain telescope and a circle-to-line imaging optic (CLIO) device. Two telescopes are required to form a wind vector since the telescopes have no azimuth adjustment. The same volume of the atmosphere is viewed from orthogonal viewpoints about 9 minutes apart. The four telescopes permit vector winds to be measured along two tracks on either side of the spacecraft. This has the advantage of allowing two local times to be sampled at the same latitude for low and mid latitudes while also providing complete pole to pole coverage.
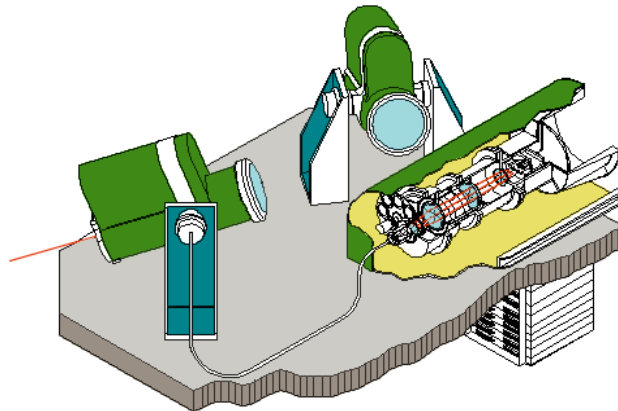

Figure 1. TIDI layout showing two of the four telescopes, the fiber optic connecting the telescopes and profiler and the electronics box.

The optical concept of the profiler is shown in Figures 2 and 3. Figure 2a shows a basic imaging system. One lens (in reality a set of lenses) collimates light from the object while a second lens (in reality a Cassegrain telescope) images the object. The magnification of the system is simply the ratio of the focal lengths of the imaging and collimating lenses. In Figure 2b the effect of adding a Fabry-Perot etalon between the two lenses is illustrated. If the image consists of light from a nearly monochromatic light source, then the image field will be modulated by the Fabry-Perot fringe pattern. Light will be passed through the etalon when the resonance condition is met ($2t\cos\theta/\lambda$=integer; t=gap thickness, θ the angle of incidence, and λ the wavelength of light) and reflected for other conditions. If the input field is large enough a series of rings, corresponding to different orders of the etalon will be observed. By designing the input fiber optics correctly it is possible to stack fibers from the 5 fields (4 telescopes, 1 calibration) so that each field projects to slightly more than one order through the etalon. If, instead of a full circle, a 90 degree segment of the circle is used as the input, then Figure 2c will result. This 90 degree segment is suitable for use with the circle-to-line imaging optic (CLIO),[5] which images the circle segment into a wedge on the CCD as shown in Figure 3. This optical design has several advantages:

- The simultaneous imaging of all telescopes on the detector allows for a significant multiplexing advantage.

- The use of a CCD provides a much larger collection efficiency that the image plane detectors used by both DE-FPI and HRDI/UARS.

- The CLIO allows efficient use of the CCD, allowing for on-chip integration of the signal which improves the duty cycle by reducing the time required to read the chip and reduces the read noise by reducing the number of reads necessary.
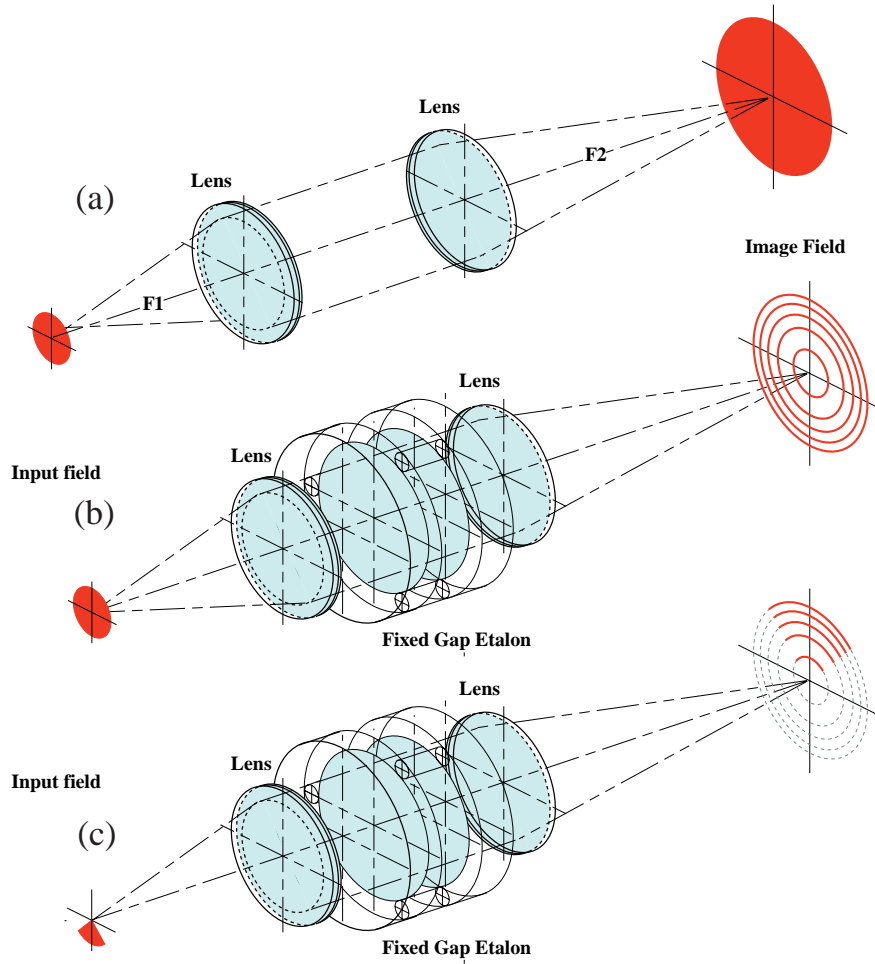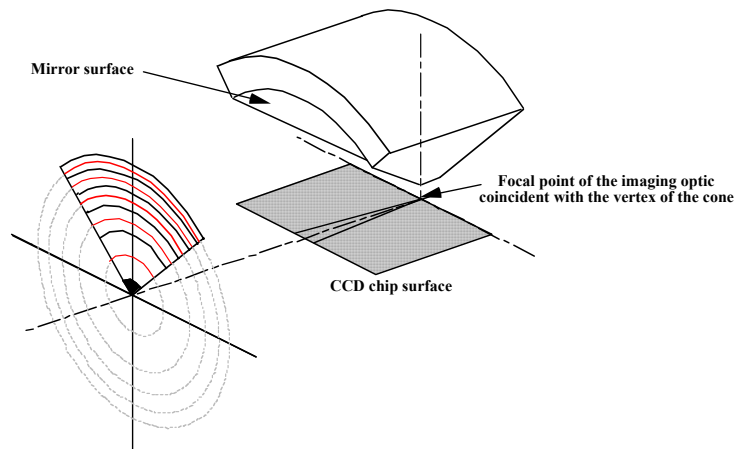

Figure 2. TIDI profiler optical concept.

Figure 3. Conversion of the Fabry-Perot fringe pattern by the CLIO.

3. DESCRIPTION OF OPTICAL COMPONENTS

3.1 Telescope

The four TIDI telescopes were constructed by the Applied Physics Laboratory (APL) of Johns Hopkins University. Table 2 summarizes the major characteristics of the telescopes. Optically, two of the most important telescope characteristics are the transmission and field of view. Figure 4 shows the measured and calculated transmission of the telescope as a function of wavelength. The calculated values were determined by using the optical properties of the gold coating. The two curves are in excellent agreement. Figure 5 shows the field of view map of the TIDI telescopes. The map is very close to the predicted field of view based on ray tracing the optics. Figure 6 shows the field of view once it is integrated in the horizontal direction, thus giving the vertical distribution of the light intensity. The full width at half height is ~0.056 degrees, very close to the desired value.

Table 2. Summary of the TIDI telescope parameters

Parameter	Value
Type	Off-axis Gregorian
Clear aperture	7.5 cm
Focal length	17.0 cm
f number	2.27
Nominal horizontal field of view	2.5 degrees
Nominal vertical field of view	0.05 degrees
Scan range	$\pm5^{o}$ from nominal 20.35° below horizon
Maximum off-axis angle to view primary	11.5 degrees
Primary coating	gold
Surface roughness	2.6 nm
Cleanliness level	less than 450
Mass	~3.8 kg (each)

TIDI telescope 3 transmittance
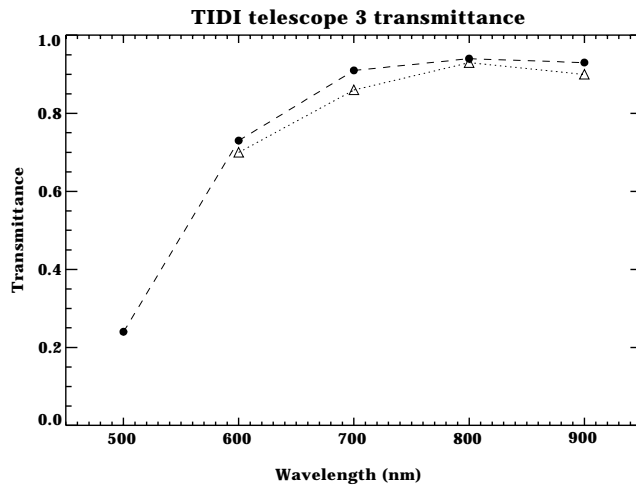
Dot, dashed line = measured; Triangle, dotted line = expected

File tele_3_trans.ps
plotted by WRS on 11-May-1999

Figure 4. Actual and expected telescope transmission.

TIDI telescope 4 field of view
Temperature: -19.5
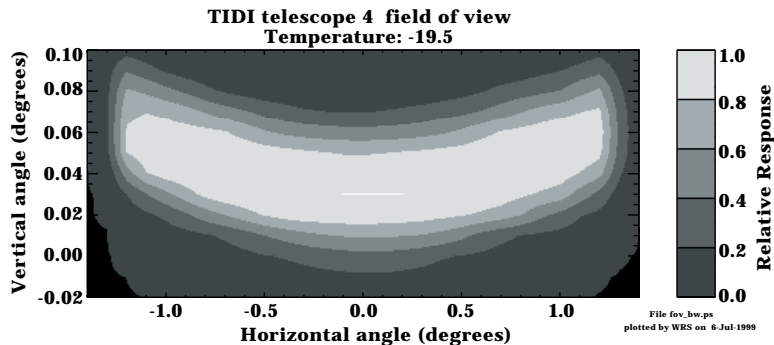
File fov_bw.ps
plotted by WRS on 6-Jul-1999

Figure 5. Approximate field of view map of TIDI telescope 4.
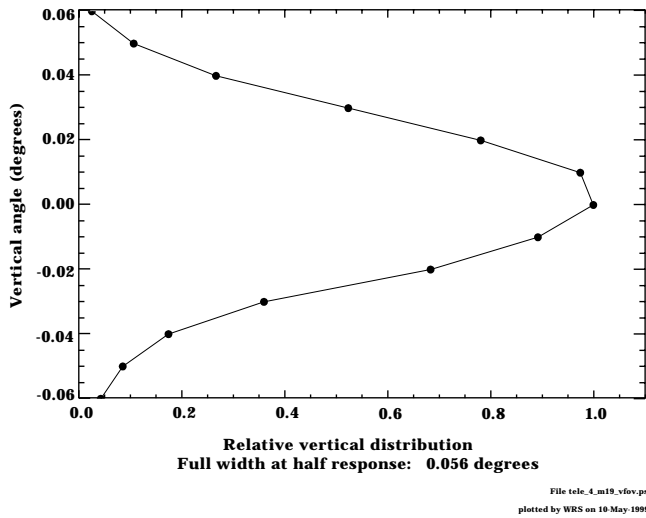
Figure 6. Vertical distribution of the TIDI telescope field of view.

TIDI fiber optics transmittance

Fields: Plus sign=1, Star=2, Diamond=3, Triangle=4, Dot=5
Area losses are included

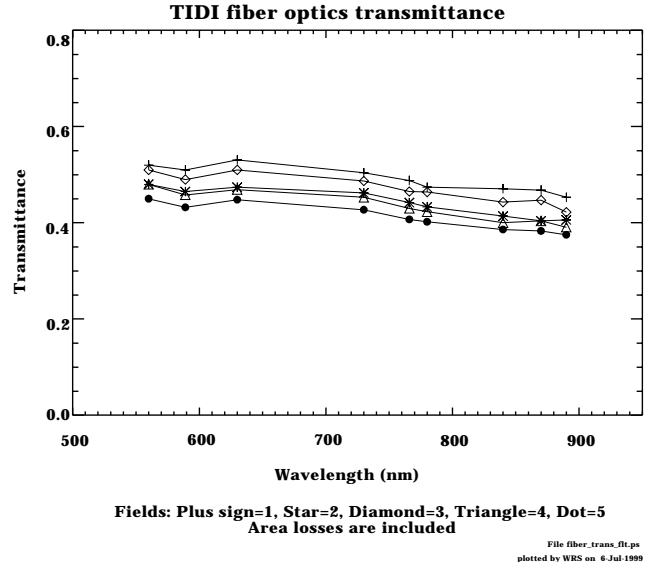File fiber_trans_flt.ps
plotted by WRS on 6-Jul-1999

Figure 7. Approximate transmission of the fiber bundle. The transmittance value includes the area loss due to the cladding and the packing of the fibers.

3.2. Fiber Optic

The fiber optic bundle connects the telescopes and calibration deck with the profiler. The main optical concerns are the number of broken fibers, the transmission of the bundle, and how well the fibers are randomized from the telescope end to the profiler end. It is important that this randomization be well done since the design of TIDI requires that the end of the fiber bundle be focused on the detector. The randomization was performed by Dolan Jenner during the construction of the fiber bundle using a proprietary process. TIDI is different from the DE-FPI and HRDI instruments which only imaged a single field on the detector for which the input need not be well focused. Figure 7 shows the approximate transmission of the fiber bundle for each of the telescope fields. The transmittance is difficult to measure and there is some uncertainty in the absolute value, but the wavelength dependence is reliable. For an individual fiber, the ratio of core area to total area is 0.51 and with a packing density of ~0.88, the expected transmittance of a fiber bundle should be about 0.45. This prediction is in good agreement with the measurements and indicates the transmission of an individual fiber is quite high. Figure 8 shows images of both ends of the fiber optic bundle. There are very few broken fibers visible (10% broken fibers would have been acceptable) indicating a high quality manufacturing process. The fiber optics parameters are summarized in Table 3.

Table 3. Fiber optics summary

Parameter	Value
Material (core and cladding)	fused silica
Fiber manufacturer	Poly Micro Inc.
Bundle packaging	Dolan Jenner
Core diameter	40 microns
Cladding diameter	56 microns
Numerical aperture	0.22
Number of fibers per field	~390
Spacing between fields on profiler end (same for all fields)	50 microns

3.3. Optical Transfer Elements

The optical transfer elements consist of optics to collimate the light for passage through the filters and etalon and to image the fringe pattern onto the detector. Table 4 summarizes some of the characteristics of the optics. The collimator section is composed of refractive elements while the imaging system is reflective. It would have been desirable to make both collimating and imaging systems reflective since it is difficult to make a system totally achromatic over the range of 550-900 nm. Because it is necessary to have the light collimated twice in the inputs, once for the filters with a diameter of 3.0

cm and again for the etalon, with a diameter of 7.5 cm, it was impractical to use reflective optics on both ends. The imaging optic is a Cassegrain telescope manufactured by Speedring, Inc.

Field 1
(calibration deck)

Profiler End
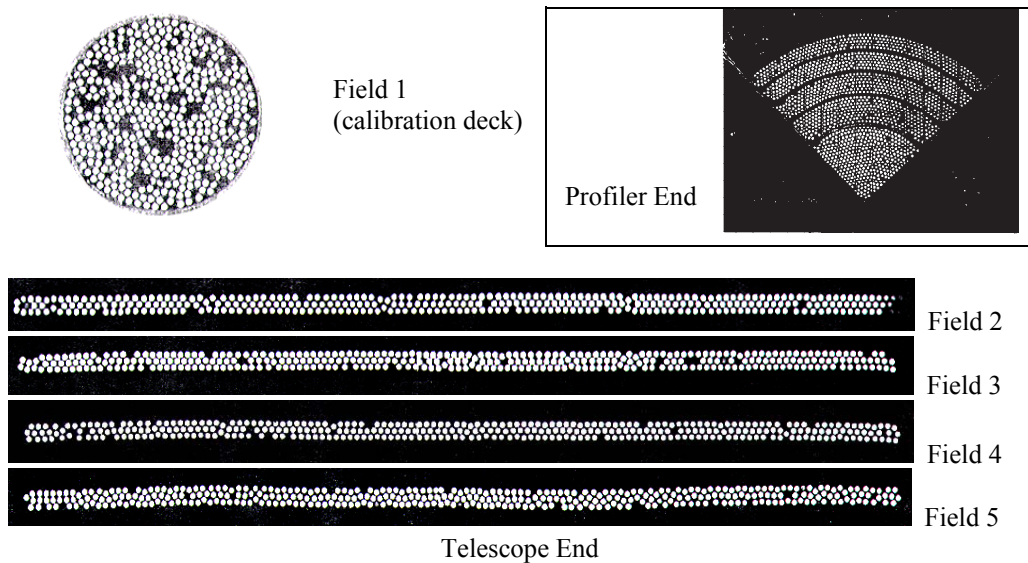
Field 2

Field 3

Field 4

Field 5

Telescope End

Figure 8. Images of the ends of fiber optic bundle. The number of broken fibers is much less than 10%. Each of the 5 fields at the profiler end are separated by a 50 micron spacer. The calibration field is nearest to the center.

Table 4. Summary of collimating and imaging optics

Parameter	Value
Filter collimator effective focal length	6.7 cm
Etalon collimator effective focal length	16.7 cm
Imaging telescope effective focal length	59.5 cm
Magnification	3.56

Table 5 shows the measured transmittances for these elements. These values are close to expected transmissions.

Table 5. Measured transmittance of optical components

Element	836 nm	786 nm	633 nm
Input collimator	0.550	0.746	0.829
Wideband blocker	0.937	0.954	0.902
Imaging optics (Speedring Cassegrain)	0.917	0.940	0.980
Product	0.473	0.669	0.732
Measured total	0.50	0.48	0.70

3.4. Image Quality

The image quality is quite important for TIDI. Not only the fringe pattern, but also the input optics need to imaged onto the detector because multiple fields are simultaneously imaged onto the detector. If the image quality is not high enough, the image will be smeared across multiple fields resulting in significant cross talk. Figure 9 shows a white light image through the system. The five fields are quite distinct with the dark areas separating them. The vertical columns in each field correspond to the rows of fibers in the input (see Figure 8). The end closest to the apex is the calibration field. The shadowing in the center of the wedge is due to a masking effect of the secondary of the imaging Cassegrain telescope. Figure 10 shows the data from Figure 9 collapsed into a single row, i.e. the signal in a column was averaged.
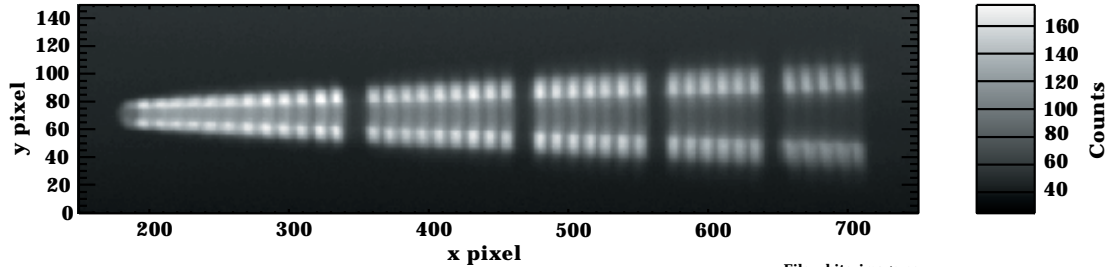
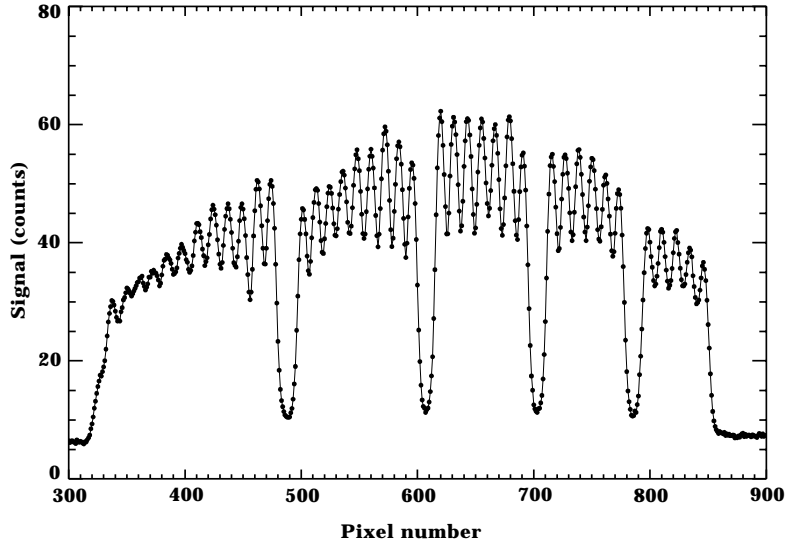Figure 9. Image of the fiber optic input onto the CCD.

Figure 10. Signal level of data in Figure 9 collapsed into a single row. The x-axis corresponds to the wavelength axis.

3.5. CCD Parameters

The TIDI CCD is a SITe model ST-005AB which is a high quantum efficiency, low noise detector. Operationally, the CCD is passively cooled to about -80°C to reduce dark signal and effects of cosmic radiation. The quantum efficiency, charge transfer efficiency (CTE), and dark current of the flight CCD are given in Table 6 and were obtained from the manufacturer (SITe) supplied test data. The parameters were verified by examining an engineering model CCD. The agreement between the measurements and data supplied by SITe was always very good. Figure 11 shows the quantum efficiency measured in the laboratory as a function of wavelength and temperature and compared to the SITe data.

Table 6. Flight CCD parameter summary

Parameter	Value
Manufacturer	SITe
Model	ST-005AB
Serial number	8165JCR18-A2
CCD size	2000 x 800 (1000 x 400 quadrant used)
Pixel size	15 x 15 microns
CTE (serial and parallel)	0.999999
Dark current@20°C	6.18 pa/cm^2, 87 e$^-$ s^{-1} pixel^{-1}
QE @400 nm@T=-80°C	70.52%
QE @500 nm@T=-80°C	74.80%
QE @600 nm @T=-80°C	67.64%
QE @700 nm @T=-80°C	76.36%
QE @800 nm @T=-80°C	62.80%
QE @900 nm @T=-80°C	36.00%
Read noise	7 e$^-$
Illumination	backside

MPP	yes	
AR coating	standard visible	
Full well capacity (parallel)	64 ke$^-$	
Full well capacity (serial)	800 ke$^-$	
Operating temperature	-80°C (passively cooled)	
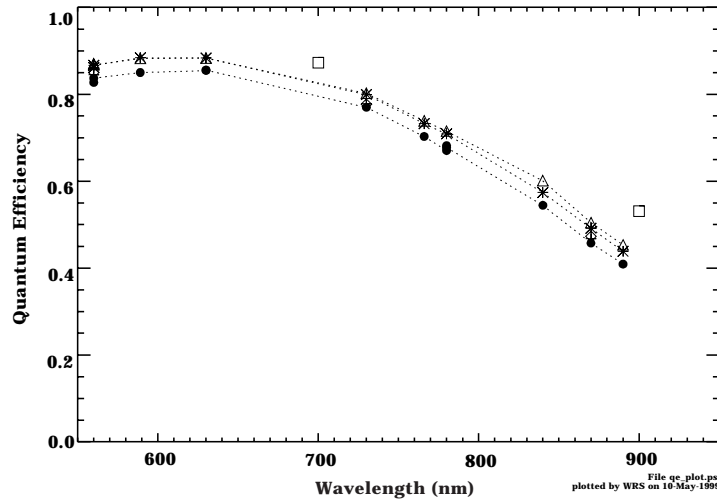
dot=T_{CCD}=-59ºC, star=T_{CCD}=-31.8ºC, plus=T_{CCD}=-53.5ºC,
diamond=T_{CCD}=-42.5ºC, triangle=T_{CCD}=-9.5ºC, square=SITE data at -45ºC

Figure 11. Measured quantum efficiency for an engineering CCD.

The TIDI CCD controller supports four gain settings for converting image data from the CCD to digital values. Table 7 shows the CCD Controller A/D converter rates, gain, and approximate bias levels for each of the gain settings. The A/D is a 12-bit system which has a range of 0-4095 counts. The four gain settings were chosen to allow a choice between a high sensitivity, relatively small dynamic range and a low sensitivity, large dynamic range. The gain of 160 e$^-$/count provides a dynamic range (6.55×10^5 e$^-$) that nearly matches that of serial register output (8×10^5 e$^-$). The gains of 5 and 10 e$^-$/count are near the read noise value of approximately 7 e$^-$/count and provide a high sensitivity with a reasonably large dynamic range. The gain of 40 e$^-$/count provides an intermediate value.

Table 7. TIDI CCD gain settings

Gain setting	Readout Rate (KHz)	System Gain (e$^-$/count)	Approximate bias level (counts)	Readout time (s)
1	64	160	10.5	0.096
2	32	40	28.5	0.100
3	8	10	120	0.111
4	4	5	253	0.126

The readout capability of the CCD is very flexible. It is possible to collect an image of any 600x50 region of any part of the working quadrant of the CCD. With this capability it is possible to examine the details of the image on the CCD. Complete images are infrequently collected for calibrations or for diagnosing problems. The readout of the CCD is relatively slow and the telemetry rate is sufficient for only 150 pixels per second. Normally, the signal is integrated on the chip. The image of the etalon forms a wedge on the CCD which is about 667 pixels in the wavelength (x) direction and a maximum of 66 pixels in the perpendicular (y) direction. The location of this wedge is determined during calibration and only this region is read out. The desired image lies in a wedge, but because of the design of the controller it is necessary to read out a rectangular region. All the pixels in the y direction are summed on the chip which reduces read noise and decreases the readout time. The binning in the x direction is under complete control of the user and it is possible to combine different numbers of pixels in the x direction. The binning can be arranged so that each readout contains nearly an equal wavelength interval. The TIDI binning pattern will divide each of the five fields of the CCD into 30 spectral channels. The innermost field (closest to the center of the fringe) will have about 166 pixels to be divided, while the outer one has only 60.

3.5. Filters

The TIDI filters isolate spectral lines for examination by the interferometer. All TIDI filters were constructed by Barr Associates. There are two filter wheels, each containing 8 filters. Since the light must pass through each wheel, one position of each contains a Schott glass OG 515 filter that has been AR coated. This transmits all wavelengths of interest to TIDI while reducing unwanted light from short wavelengths. Additional wideband blocking is provided by a filter that isolates the spectral region 550-900 nm. This filter is mounted in the collimating optics and not on the filter wheel. Figure 12 shows the transmission curve for this filter and Figure 13 shows a narrowband (0.3 nm) filter for use in the O_2 (0-0) band. The 14 filters that are designated for science investigations are summarized in Table 8. Many filters transmit calibration lines from argon, krypton, or neon which are part of the calibration system. The filters are tilted by 1 degree relative to the optical axis to direct the reflected light out of the optical path. The filters are constructed of metal oxide material which are very durable and have a low thermal drift coefficient. The thermal drifts are about a factor of 10 lower than the filters used by DE-FPI and HRDI/UARS. This reduces the requirement for instrument control significantly. The requirement for the TIDI instrument is $\pm 5^{o}C$ about a nominal operating temperature of $20^{o}C$.
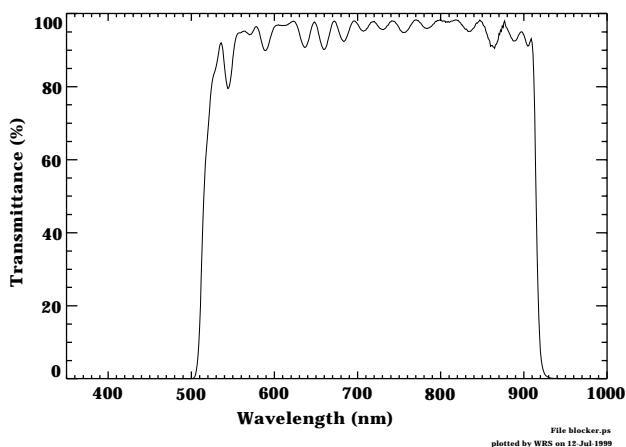

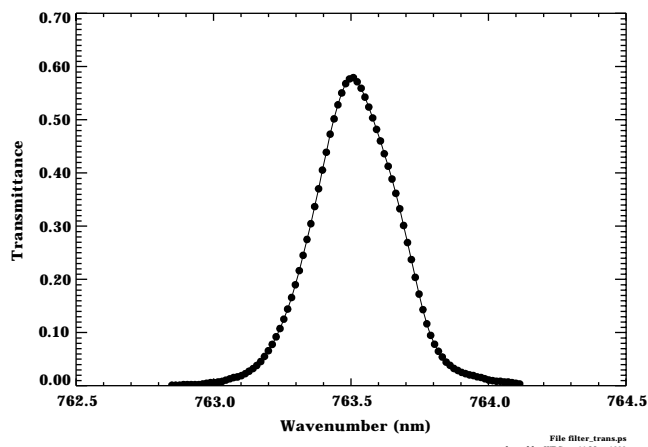Figure 12. Transmission curve for wideband blocker

Figure 13. Measured transmission curve for a narrow band O_2 (0-0) filter.

Table 8. TIDI filter summary

Filter wheel and position	Filter center wavelength (in air) (nm)	Emissions	Bandwidth (full width half maximum) (nm)	Peak transmittance
1-1	867.13	$O_2(^1\Sigma)$ (0-1) P11 pair and argon (866.79 nm)	0.35	0.56
1-2	763.62	$O_2(^1\Sigma)$ (0-0) P9 pair and argon (763.51 nm)	0.32	0.62
1-3	557.89	OI (^{1}S)	0.55	0.85
1-4	OG 515	short wavelength blocker		
1-5	630.23	OI (^{1}D) and neon (630.48 nm)	0.62	0.77
1-6	765.20	$O_2(^1\Sigma)$ (0-0) P15 pair	0.30	0.70
1-7	866.14	$O_2(^1\Sigma)$ (0-1) P7 pair and argon (866.79 nm)	0.36	0.57
1-8	892.01	OH Meinel (7-3) P1(3) pair and neon (891.95 nm)	0.55	0.76
2-1	OG 515	short wavelength blocker		
2-2	732.04	OII (^{2}P) pair	0.58	0.58
2-3	844.70	OI triplet	0.61	0.67
2-4	557.28	OI (^{1}S) cal filter krypton (557.03 nm)	0.65	0.53
2-5	589.37	NaD doublet and neon (590.25 nm)	1.01	0.61
2-6	779.60	OH Meinel (9-4) P1(2) pair	0.73	0.71
2-7	763.92	$O_2(^1\Sigma)$ (0-0) P branch	3.95	0.79

		and argon (763.51 nm)		
2-8	760.51	$O_2(^1\Sigma)$ (0-0) R branch	1.92	0.81
		and krypton (760.15 nm)		

3.7. CLIO Cone

The CLIO cone converts the fringe pattern to a relatively narrow wedge on the CCD. It has an apex angle of 45 degrees and extends 180 degrees. Only 90 degrees are used optically, with the material in the rest of the cone providing radiation shielding for the CCD. The cone is constructed from aluminum and overcoated with nickel. This was diamond turned to a finish with an rms roughness of about 3 nm. No polishing of the surface was performed. The surface was overcoated with Denton FSS-99 coating which is a silver and dielectic coating and gives the cone a reflectivity of greater than 95% throughout the region of interest.

3.8. Etalon

The etalon is the spectrally resolving element of the interferometer. Optically, the TIDI etalon was optimized for mesospheric wind observations using the O_2 Atmospheric (0,0) band around 762 nm. The optimization procedure specified a gap thickness of 2.2 cm and the reflectivity of about 80%. The actual reflectivity curve is shown in Figure 14. The etalon requires a 7.5 cm clear aperture to accept the light from all four telescopes and the calibration field. The etalon is constructed out of fused silica and the posts are made of zerodur. This is the same as the DE-FPI etalon and the fixed etalon of HRDI/UARS. Similar to DE-FPI, but unlike HRDI/UARS which used optical contacts, the posts are cemented to the plates with about a 1-micron thick layer of Norland 61 UV setting epoxy. The mount is similar to the design used by DE-FPI.[6,7] The etalon characteristics are summarized in Table 9.

Table 9. Etalon parameter summary

Parameter	Value
Plate material	fused silica (Supersil-B)
Post material	zerodur
Plate diameter	10.5 cm
Coated area diameter	8.6 cm
Back surface wedge angle	0.9 degree
Plate thickness	2.54 cm
Post length	2.2 cm
Post to plate contact	~1 micron thick epoxy layer
	(Norland 61) (no optical contact)

File tidi_reft.ps
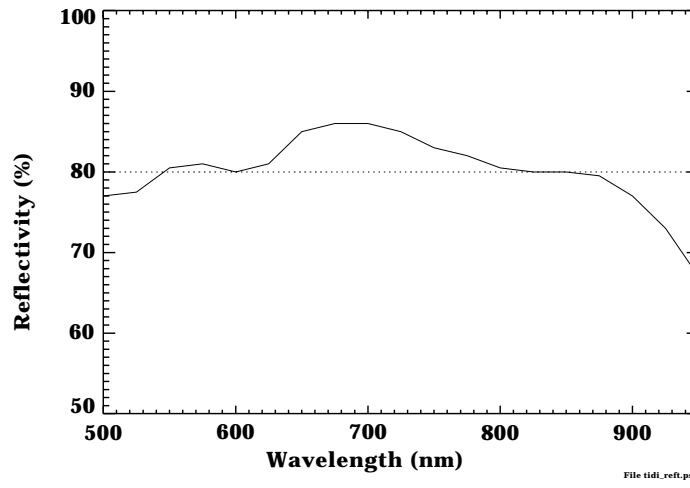plotted by WRS on 7-Jul-1999

Figure 14. Measured reflectivity of the TIDI etalon plates.

4. SYSTEM CHARACTERISTICS

4.1. Spectral Resolution

An image of the interference pattern of a frequency stabilized helium neon laser is shown in Figure 15. The x scale is non-linear in wavelength so the fringes at the left side of the image (smaller pixel numbers) appear broader. This test configuration filled more of the CCD than will be used operationally, and only the first seven orders (counting from the left) are used operationally. Figure 16 shows the data collapsed into a single line, remapped so the x axis is linear with wavelength. The derived finesses are slightly lower than hoped for, but still acceptable. Other tests (not shown here) demonstrate the finesse increases at longer wavelengths, consistent with plate distortions being a major component of the overall finesse.
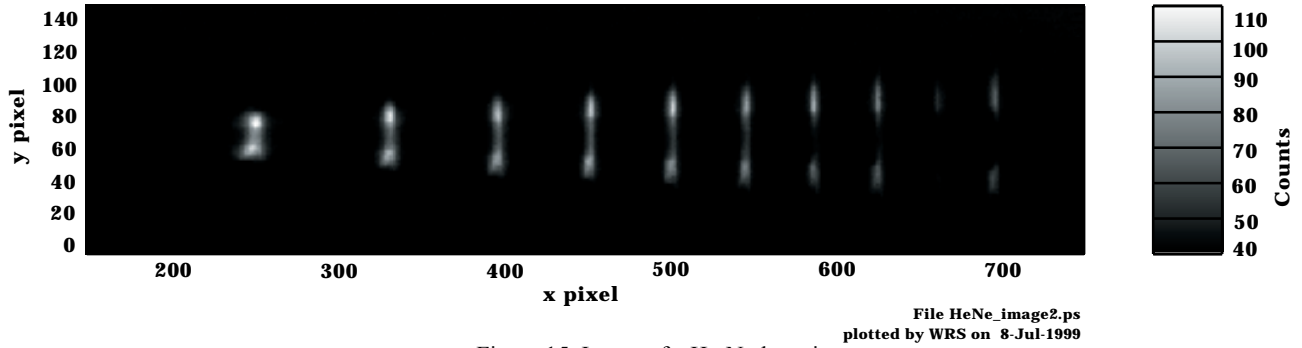

File HeNe_image2.ps
plotted by WRS on 8-Jul-1999

Figure 15. Image of a He-Ne laser input.

File tidi_etalon_finesse2.ps
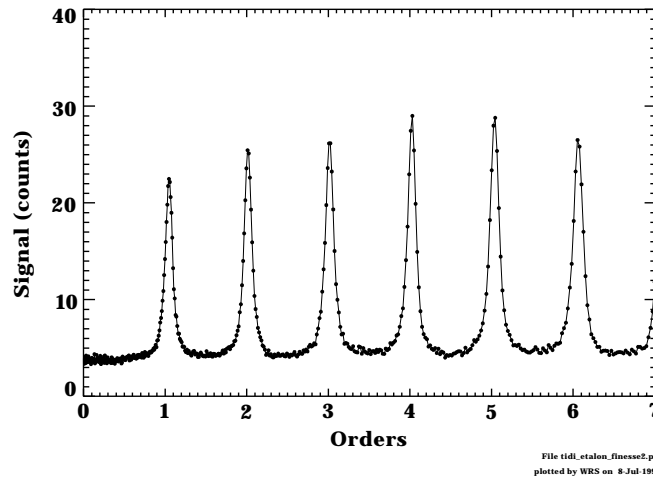plotted by WRS on 8-Jul-1999

Figure 16. He-Ne laser light mapped so the x axis is linear in wavelength. The data used filled more of the CCD than actually used in normal operations so only the first 7 orders provide meaningful finesse values.

4.2. Estimated Sensitivity

The TIDI calibrations are not complete at the time of this writing so the final sensitivity numbers for the instrument are not available. Using the values presented in the previous sections it is possible to estimate the throughput and sensitivity to Doppler shifts. Here a simplified form of the TIDI instrument function is presented to illustrate how the various parameters discussed in the previous sections contribute to the overall instrument performance. The signal, C, on any spectral channel, j, can be expressed as the convolution of the Fabry-Perot transmission function and the illumination source multiplied by appropriate throughput factors:

$$C(j) = S\left(\frac{1-R}{1+R}\right)\Delta t\left\{1 + 2\sum_{n=1}^{\infty} R^n \exp\left\{-4\pi^2 n^2 t^2 \alpha_D^2 - \frac{\pi^2 n^2}{4N_D^2 \ln 2}\right\} \operatorname{sinc}\left(\frac{\pi n}{N_A}\right) \operatorname{sinc}\left(\frac{\pi n}{N_{FOV}}\right) \cos\left\{2\pi n\left\{\frac{j}{N_A} - \phi\right\}\right\}\right\} \quad (1)$$

where Δt is the integration time, ϕ is a phase term which locates the position of the fringe peak on the detector (the wind information is in this term) and the other terms are defined in Tables 10 and 11. The sensitivity, S, is given by

$$S(\lambda) = \frac{A\Omega 10^6}{4\pi n_{chan}} T_{tele}(\lambda) T_{fiber}(\lambda) T_{coll}(\lambda) T_{wb}(\lambda) T_{fil}(\lambda) T_{im}(\lambda) R_{cone}(\lambda) Q(\lambda) T_{m\,arg\,in} \qquad (2)$$

where k is the gain (Table 7). This formulation assumes that the area-solid angle product for all channels is the same, which is only an approximation since the number of CCD pixels per channel must be an integer. The 1/e width of a spectral line is given by

$$\alpha_D = 4.30 \times 10^{-7} \nu_o \left(\frac{T}{M}\right)^{1/2} \qquad (3)$$

where ν_o is the central wavenumber, T is the emitter temperature and M is the atomic mass.

The aperture finesse is the number of channels used to cover a free spectral range of the etalon. The aperture finesse varies slightly with channel number because of the discreteness of the CCD pixels, but to a good approximation can be expressed as a constant across the field. The optical system was designed so that 1.2 orders covered 30 spectral channels at 900 nm. The aperture finesse at any other wavelength is

$$N_A(\nu) = N_A(\nu_o)\frac{\nu_o}{\nu} = N_A(\lambda_o)\frac{\lambda}{\lambda_o} \qquad (4)$$

which gives nearly 2 orders at 557 nm. A minimum of 1.2 orders was chosen to be sure the line was well defined even if it was near the edge of the field. Since the TIDI etalon is a fixed gap etalon, there is no way to adjust the line position.

The defect finesse is caused by distortion of the plates. This is particularly important for a spaceflight etalon since it must be held securely during launch to prevent breaking. This requires a firm mounting which can significantly distort the plates. The defect finesse has not been evaluated for TIDI, but it is expected that the overall instrument finesse will be about 10, and the modeling presented here assumes a corresponding defect finesse. The defect finesse (whatever its exact form) has a linear scaling factor with wavelength

$$N_D(\nu) = N_D(\nu_o)\frac{\nu_o}{\nu} = N_D(\lambda_o)\frac{\lambda}{\lambda_o}. \qquad (5)$$

The field of view finesse is the spectral broadening caused by the differing spacecraft velocity motion component from one end of the field of view to the other. This causes a varying Doppler shift across the field. The light is spatially scrambled by the fiber bundle and this effect acts as a broadening of the fringe. In order to calculate it properly, field of view maps such as shown in Figure 5 must be numerically integrated. To provide an estimate of the effect, a rectangular field of view is assumed with uniform contributions from all locations in the field. In that case a field of view finesse can be defined by

$$N_{FOV} = \frac{c}{2t\nu_o v_{sat}\cos\theta_{dep}\sin\theta_{az}\Delta\theta_{az}}. \qquad (6)$$

Tables 10 and 11 show the values that allow the throughput and finesse to be calculated for representative wavelengths through the TIDI operating range. Also shown in Table 11 is the Doppler shift error for a 10-kR line viewed for 1 s. This is not intended to be representative of the TIDI errors, but to show for a given input how the errors will vary due to changing wavelengths and different emissions.

5. CONCLUSION

This paper has briefly described the TIDI optical design and the performance of some of the optical components. The TIDI design is very efficient, using the light from all 4 telescopes simultaneously, using high quality optical components and a high sensitivity CCD detector. The analysis of the characteristics of the elements indicate that TIDI will able to fully meet the scientific goals. Further information on the TIMED program and TIDI project can be obtained from the web sites http://www.sprl.umich.edu/TIDI and http://www.timed.jhuapl.edu.

6. ACKNOWLEDGMENTS

Table 10. TIDI estimated transmittance and throughput parameters

Parameter	550 nm	630 nm	760 nm	860 nm	890 nm
Telescope diameter (cm)	7.5	7.5	7.5	7.5	7.5
Telescope effective area (cm^2) (A)	44.2	44.2	44.2	44.2	44.2
Field of view (degrees)	2.5 x 0.05	2.5 x 0.05	2.5 x 0.05	2.5 x 0.05	2.5 x 0.05
field of view (sr) (Ω)	3.81 x 10^{-5}	3.81 x 10^{-5}	3.81 x 10^{-5}	3.81 x 10^{-5}	3.81 x 10^{-5}
Telescope area - field of view product (cm^2 sr)	1.68x10^{-3}	1.68x10^{-3}	1.68x10^{-3}	1.68x10^{-3}	1.68x10^{-3}
Telescope transmittance (T_{tele})	0.49	0.78	0.93	0.93	0.93
Fiber optic transmittance (T_{fiber})	0.49	0.49	0.45	0.42	0.41
Collimator transmittance (T_{coll})	0.87	0.83	0.76	0.53	0.51
Wide band blocker transmittance (T_{wb})	0.90	0.90	0.95	0.92	0.91
Filter peak transmittance (T_{fil})	0.85	0.77	0.62	0.56	0.76
Imaging optics transmittance (T_{im})	0.98	0.98	0.95	0.91	0.90
CLIO cone reflectivity (R_{cone})	0.95	0.95	0.95	0.95	0.95
Factor for other transmission losses (T_{margin})	0.75	0.75	0.75	0.75	0.75
Optics transmittance (T_{opt})	0.11	0.15	0.13	0.07	0.09
Detector quantum efficiency (Q)	0.71	0.70	0.68	0.47	0.39
number of detector channels per field, (n_{chan})	30	30	30	30	30
Sensitivity (e$^-$ s^{-1} channel^{-1} R^{-1}) (S)	0.47	0.64	0.51	0.20	0.23

Table 11. Estimated spectral properties of the TIDI interferometer system

Parameter	550 nm	630 nm	760 nm	860 nm	890 nm
Etalon gap spacing (t)	2.2 cm	2.2 cm	2.2 cm	2.2 cm	2.2 cm
Reflectivity, (R)	0.805	0.818	0.826	0.798	0.780
Reflectivity finesse N_R	14.5	15.6	16.4	13.9	12.6
Number of orders on detector for each field	2.0	1.7	1.4	1.3	1.2
Aperture finesse (spectral channels/order) (N_A)	15.3	17.5	21.1	23.9	24.7
Defect finesse (N_D)	18.3	21.0	25.3	28.7	29.7
Satellite speed (v_{sat})	7500 ms^{-1}	7500 ms^{-1}	7500 ms^{-1}	7500 ms^{-1}	7500 ms^{-1}
Depression angle from horizontal (θ_{dep})	21°	21°	21°	21°	21°
Azimuth angle from velocity vector(θ_{az})	45°	45°	45°	45°	45°
Horizontal field width $\Delta\theta_{az}$	2.5^o	2.5^o	2.5^o	2.5^o	2.5^o
Field of view finesse (N_{FOV})	17.3	19.9	24.0	27.1	28.1
Total finesse	8.0	8.9	9.9	9.3	8.9
Etalon peak transmittance	0.66	0.67	0.72	0.80	0.83
Emitter	O	O	O_2	O_2	OH
Atomic mass, (M)	16	16	32	32	18
Representative temperature (T)	200 K	1000 K	180 K	180 K	180 K
1/e linewidth (α_D)	0.028 cm^{-1}	0.054 cm^{-1}	0.013 cm^{-1}	0.012 cm^{-1}	0.015 cm^{-1}
Error for 10kR line brightness	4.7 ms^{-1}	7.9 ms^{-1}	4.9 ms^{-1}	7.8 ms^{-1}	8.7 ms^{-1}

7. REFERENCES

1. J.-H. Yee, G. E. Cameron, and D. Y. Kusnierkiewicz, "An Overview of TIMED," *SPIE 3756* (this issue), 1999.
2. P. B. Hays, T. L. Killeen, and B. C. Kennedy, "The Fabry-Perot Interferometer on Dynamics Explorer," *Space Sci. Instrumentation 5*, pp. 395-416, 1981.
3. P. B. Hays, V.J. Abreu, M.E. Dobbs, D.A. Gell, H.J. Grassl, and W.R. Skinner, "The High Resolution Doppler Imager on the Upper Atmosphere Research Satellite," *J. Geophys. Res. 98*, pp. 10,713-10,723, 1993.
4. H. J. Grassl, W. R. Skinner, P. B. Hays, M. D. Burrage, D. A. Gell, A. R. Marshall, D. A. Ortland, and V. J. Abreu, "Atmospheric wind measurements with the High Resolution Doppler Imager (HRDI)," *J. Spacecraft & Rockets 32*, No. 1, pp. 169-176, Jan.-Feb. 1995.
5. P. B. Hays, "Circle to line interferometer optical system," *Appl. Opt. 29*, pp. 1482-1489, 1990.
6. T. K. Killeen, P. B. Hays, B. C. Kennedy, and D. Rees, "Stable and rugged etalon for the Dynamics Explorer Fabry-Perot interferometer. 2: Performance," *Appl. Opt. 21*, pp. 3903-3912, 1982.
7. D. Rees, T. J. Fuller-Rowell, A. Lyons, T. L. Killeen, and P. B. Hays, "Stable and rugged etalon for the Dynamics Explorer Fabry-Perot interferometer. 1: Design and construction," *Appl. Opt. 21*, pp. 3896-3902, 1982.